View metadata, citation and similar papers at core.ac.uk

brought to you by CORE

provided by ScholarlyCommons@Penn

University of Pennsylvania
ScholarlyCommons

Departmental Papers (MEAM)

Department of Mechanical Engineering & Applied Mechanics

2011

When MHD-Based Microfluidics is Equivalent to Pressure-Driven Flow

Mian Qin
University of Pennsylvania, qq1985ear@gmail.com

Haim H. Bau
University of Pennsylvania, bau@seas.upenn.edu

Follow this and additional works at: http://repository.upenn.edu/meam_papers


Part of the Applied Mechanics Commons

Recommended Citation

Qin, Mian and Bau, Haim H., "When MHD-Based Microfluidics is Equivalent to Pressure-Driven Flow" (2011). *Departmental Papers (MEAM)*. 304.
http://repository.upenn.edu/meam_papers/304

Mian Qin and Haim H. Bau, 2011, When MHD-Based Microfluidics is Equivalent to Pressure-Driven Flow, Micro and Nano Fluidics 10, (2), 287-300 (DOI: 10.1007/s10404-010-0668-2)

This paper is posted at ScholarlyCommons. http://repository.upenn.edu/meam_papers/304
For more information, please contact libraryrepository@pobox.upenn.edu.

When MHD-Based Microfluidics is Equivalent to Pressure-Driven Flow

Abstract
Magnetohydrodynamics (MHD) provides a convenient, programmable means for propelling liquids and controlling fluid flow in microfluidic devices without a need for mechanical pumps and valves. When the magnetic field is uniform and the electric field in the electrolyte solution is confined to a plane that is perpendicular to the direction of the magnetic field, the Lorentz body force is irrotational and one can define a "Lorentz" potential. Since the MHD-induced flow field under these circumstances is identical to that of pressure-driven flow, one can utilize the large available body of knowledge about pressure-driven flows to predict MHD flows and infer MHD flow patterns. In this note, we prove the equivalence between MHD flows and pressure-driven flows under *certain* conditions other than flow in straight conduits with rectangular cross-sections. We determine the velocity profile and the efficiency of MHD pumps, accounting for current transport in the electrolyte solutions. Then, we demonstrate how data available for pressure driven flow can be utilized to study various MHD flows, in particular, in a conduit patterned with pillars such as may be useful for liquid chromatography and chemical reactors. Additionally, we examine the effect of interior obstacles on the electric current flow in the conduit and show the existence of a particular pillar geometry that maximizes the current.

Keywords
Magneto-Hydrodynamics, Microfluidics, Liquid Chromatography, Lorentz Force, Nernst-Planck equations, MHD

Disciplines
Applied Mechanics | Engineering | Mechanical Engineering

Comments
Mian Qin and Haim H. Bau, 2011, When MHD-Based Microfluidics is Equivalent to Pressure-Driven Flow, Micro and Nano Fluidics 10, (2), 287-300 (DOI: 10.1007/s10404-010-0668-2)

This journal article is available at ScholarlyCommons: http://repository.upenn.edu/meam_papers/304

Mian Qin and Haim H. Bau, 2011, When MHD-Based Microfluidics is Equivalent to Pressure-Driven Flow, Micro and Nano Fluidics 10, (2), 287-300 (DOI: 10.1007/s10404-010-0668-2)

When MHD-Based Microfluidics is Equivalent to Pressure-Driven Flow

Mian Qin and Haim H Bau*

Department of Mechanical Engineering and Applied Mechanics,
University of Pennsylvania, Philadelphia PA 19104 USA
* Corresponding author: bau@seas.upenn.edu

Abstract

Magnetohydrodynamics (MHD) provides a convenient, programmable means for propelling liquids and controlling fluid flow in microfluidic devices without a need for mechanical pumps and valves. When the magnetic field is uniform and the electric field in the electrolyte solution is confined to a plane that is perpendicular to the direction of the magnetic field, the Lorentz body force is irrotational and one can define a "Lorentz" potential. Since the MHD-induced flow field under these circumstances is identical to that of pressure-driven flow, one can utilize the large available body of knowledge about pressure-driven flows to predict MHD flows and infer MHD flow patterns. In this note, we prove the equivalence between MHD flows and pressure-driven flows under *certain* conditions other than flow in straight conduits with rectangular cross-sections. We determine the velocity profile and the efficiency of MHD pumps, accounting for current transport in the electrolyte solutions. Then, we demonstrate how data available for pressure driven flow can be utilized to study various MHD flows, in particular, in a conduit patterned with pillars such as may be useful for liquid chromatography and chemical reactors. Additionally, we examine the effect of interior obstacles on the electric current flow in the conduit and show the existence of a particular pillar geometry that maximizes the current.

Keywords

Magneto-Hydrodynamics • Microfluidics • Liquid Chromatography • Lorentz Force • Nernst-Planck equations

List of Symbols

$\mathbf{b}$	Magnetic field	*Tesla*
c_i	Concentration of species i	mol/m^3
C_p	Specific heat	$J/kg \cdot K$
D_i	Diffusion coefficient	m^2/s
E	Electric field	*V/m*
eff	Pumping efficiency	
$\mathbf{f}_{\nabla B}$	Magnetophoretic body force	N/m^3
$\mathbf{f}_E$	Electrostatic body force	N/m^3
$\mathbf{f}_L$	Lorentz body force	N/m^3
H	Conduit height	*m*
h	Convective heat transfer coefficient	W/m^2-K
Ha	Hartmann number	
I	Electric current	*A*
$\mathbf{j}$	Electric current density	A/m^2
j_e	Exchange current density	A/m^2
j_0	Current density scale	A/m^2
K	Lorentz force to viscous force ratio	
L	Conduit length	*m*
m	Integration constant	
$\mathbf{N}_i$	Ion flux of species i	$mol/(m^2 \cdot s)$

p	Pressure	Pa
Q	Flow rate	m^3 / s
R	Gas constant	$J / (K \cdot mol)$
R_H	Hydraulic resistance	$Pa \cdot s / m^4$
Re	Reynolds number	
Re_m	Magnetic Reynolds number	
W	Conduit width	m
α	Charge transfer coefficient	
υ	Magnetic diffusivity	m^2 / s
μ	Fluid viscosity	$Pa \cdot s$
λ	Drag coefficient	
η	Overpotential	$Volt$
Δp_{stall}	Stall pressure	Pa
T	Temperature	K
$\mathbf{u}$	Velocity field	m / s
$\overline{u}$	Average fluid velocity	m / s
z_i	Valence	
ϕ	Electric potential	V
ε_s	dielectric permittivity	F / m
ν_i	Ion mobility	$m^2 / (Volt \cdot s)$
σ_{ionic}	Ionic conductivity	$ohm^{-1} m^{-1}$
ς_0	Magnetic permeability	N / A^2
Ξ	Magnetic potential	N / m^2

χ_m	Molar magnetic susceptibility	m^3 / mol

1 Introduction

A lab-on-a-chip (**LOC**) device is a minute chemical processing plant that integrates on a single substrate common laboratory processes ranging from filtration and mixing to separation and detection. To achieve these tasks, it is often necessary to propel and stir liquids and control fluid flow. Since, in many applications, one uses solutions that are electrically conductive, one can transmit electric currents through these solutions. When the device is subjected to an external magnetic field provided by either permanent magnets or electromagnets, the electric current interacts with the magnetic field to produce Lorentz body forces, which, in turn, drive fluid motion. This phenomenon is commonly referred to as magneto-hydrodynamics and has been utilized, among other things, to pump fluids in microfluidic conduits (Qian and Bau 2005; Jang and Lee 2000; Lemoff and Lee 2000; Leventis and Gao 2001; West *et al.* 2002 and 2003; Zhong *et al.* 2002; Eijkel *et al.* 2003; Bao and Harrison 2003a and 2003b; Arumugam *et al.* 2005 and 2006; Aguilar *et al.* 2006; Nguyen and Kassegne 2008), control fluid flow in microfluidic networks without a need for mechanical pumps and valves (Bau *et al.* 2003); stir and mix fluids (Bau *et al.* 2001; Yi *et al.* 2002; Xiang and Bau 2003; Qian and Bau 2005; Gleeson and West 2002; West *et al.* 2003; Gleeson *et al.* 2004); and enhance mass transfer next to electrodes' surfaces (Boum and Alemany 1999; Lioubashevski *et al.* 2004; Alemany and Chopart 2007). For a recent review of a few applications of MHD in microfluidics, see Qian and Bau (2009).

Most of the literature pertaining to MHD focuses on liquid metals and ionized gases (Davidson 2001). In contrast, in microfluidic applications, one typically deals with electrolyte solutions. The modeling of MHD flows of electrolyte solutions differs from that of liquid metals since the local electric conductivity is a function of the electrolytes' concentration, which, in turn, depends on the flow field. Nernst-Plank equations for the ions' flux (Newman 1991), the Navier-Stokes momentum equation (Batchelor 1967), and Maxwell's equations for the magnetic field need to be solved concurrently. Additionally, one often needs to consider non-linear electrode kinetics and the possible production of undesirable products of electrochemical reactions at the electrodes' surfaces. Another potential undesired phenomenon is electrophoretic migration of charged molecules and particles in the electric fields induced by the electrodes.

Fortunately, for electrolytes with low magnetic permittivity and a low magnetic Reynolds number, the determination of the magnetic field can be decoupled from that of the ion concentration, fluid flow, and electric fields. Furthermore, electric current induction can be neglected.

The typical MHD pump consists of an electrolyte-filled conduit with a rectangular cross-section whose opposite walls are coated with electrodes. It has long been known that when the electrolytes are subjected to a uniform magnetic field directed parallel to the electrodes' surfaces, the MHD flow is equivalent to pressure-driven flow (Ho 2007). We show that this equivalence also exists in some other circumstances that are common in microfluidic systems. We utilize the equivalence between MHD-driven flow and pressure-driven flow to obtain the flow patterns of MHD flow in conduits patterned with pillar arrays. Such conduits can serve as chromatographic and separation columns and as catalytic reactors. The pillars provide increased surface area and solid support for stationary phases and catalytic surfaces (to facilitate and enhance heterogeneous reactions). MHD–driven flow is of particular interest to chromatography as it allows one to drive fluid flow in a closed loop, in effect, providing an "infinitely long column" (Martin 1958; Eijkel *et al.* 2004). In a traditional, linear, separation column, the column length must be selected in advance, which is not always feasible when dealing with unknown analytes or with analytes that have slightly different partition coefficients. No such advance knowledge is needed in the case of the closed loop chromatograph. The closed-loop chromatograph also allows for real-time detection.

In the case of the column patterned with the pillar array, we show that when the current is controlled (known), one can deduce the MHD flow rate by using literature data available for pressure-driven flow in a similar geometry. When the potential difference between the electrodes is the control parameter, the equivalence between the pressure-driven flow and the MHD-driven flow cannot be applied directly to obtain the flow field, and we solve the coupled Nernst-Planck and Navier-Stokes equations to obtain the concentration, current, and flow fields. In the latter case, we can verify the computations by comparing our computed drag coefficients with literature data available for the pressure-driven flow.

The paper is organized as follows. Section 2 introduces the mathematical model and outlines the various assumptions that apply for the conditions typically prevailing in microfluidic systems. Section 3 proves the existence of a "Lorentz potential" under special

conditions and thus the equivalence between MHD-driven and pressure-driven flow under those conditions. Section 4 reviews briefly MHD flow in a uniform conduit. The analysis accounts for concentration gradients induced by the electric field. Additionally, we redefine the efficiency of the MHD pump energy conversion and estimate the temperature increase in the MHD pump. Section 5 studies MHD flow in a conduit patterned with a pillar array. Section 6 concludes.

2 Mathematical Model

Consider an electrolyte solution consisting of l types of ionic species with concentrations c_i $(i=1,....,l)$ subjected to external electric and magnetic fields. The mass transport of the i-th ion is described by the Nernst-Planck (**NP**) equation:

$$\frac{\partial c_i}{\partial t} = -\nabla \cdot \mathbf{N}_i \qquad (i=1,...,l), \tag{1}$$

where the mass flux of species i

$$\mathbf{N}_i = \mathbf{u}c_i - D_i \nabla c_i - z_i \nu_i F c_i (\nabla \phi - \mathbf{u} \times \mathbf{b}) \tag{2}$$

is comprised of convective, diffusive, electro-migrative, and inductive terms. In the above, $\mathbf{u}$ is the fluid velocity; D_i and $\nu_i = D_i/(RT)$ are, respectively, the diffusivity and the mobility of the i-th ion species; z_i is the valence of the i^{th} ion species; R is the gas constant; T is the absolute temperature; F is the Faraday constant; ϕ is the electric potential; and $\mathbf{b}$ is the magnetic field vector. We adopt here the convention that bold and regular letters represent, respectively, vectors and scalars.

The electric potential satisfies the Poisson equation:

$$-\nabla \cdot (\varepsilon_s \nabla \phi) = F \sum_{i=1}^{l} z_i c_i , \tag{3}$$

where ε_s is the dielectric permittivity of the solvent.

Typically, in a homogeneous solution, net charge exists only in narrow regions next to solid surfaces (electric double layers, **EDL**) and the bulk of the solution is nearly electrically neutral:

$$\sum_{i=1}^{l} z_i c_i \approx 0 . \tag{4}$$

The electric current flux is

$$\mathbf{j} = F\sum_{i=1}^{l} z_i \mathbf{N}_i = -F\sum_{i=1}^{l} z_i D_i \nabla c_i - \sigma_{ionic}(\nabla\phi - \mathbf{u}\times\mathbf{b}) , \tag{5}$$

where $\sigma_{ionic} = F^2\sum_{i=1}^{l} z_i^{\,2}\nu_i c_i$ is the ionic conductivity of the electrolyte solution.

The fluid motion satisfies the Navier-Stokes (**NS**) equation:

$$\rho\left(\frac{\partial \mathbf{u}}{\partial t} + \mathbf{u}\cdot\nabla\mathbf{u}\right) = -\nabla p + \mu\nabla^2\mathbf{u} + \mathbf{f}_{EM} , \tag{6}$$

where the electromagnetic body force

$$\mathbf{f}_{EM} = \mathbf{f}_L + \mathbf{f}_{\nabla B} + \mathbf{f}_E . \tag{7}$$

The Lorentz force

$$\mathbf{f}_L = \mathbf{j}\times\mathbf{b} ; \tag{8}$$

the magnetophoretic force (when the ions are ferromagnetic and/or paramagnetic)

$$\mathbf{f}_{\nabla B} = \frac{\chi_m}{2\varsigma_0} c_i^{(m)} \nabla\mathbf{b}^2 ; \tag{9}$$

and the electrostatic force

$$\mathbf{f}_E = F\nabla\phi\cdot\sum_{i=1}^{l} z_i c_i . \tag{10}$$

In the above, ρ and μ are, respectively, the fluid density and viscosity; $\varsigma_0 = 1.257\times10^{-6}\, N\cdot A^{-2}$ is the magnetic permeability of the vacuum; p is the dynamic pressure; χ_m is the molar susceptibility; and the subscript m denotes paramagnetic ions.

Due to the small dimensions of microfluidic conduits, we neglected buoyancy effects in equation (6). We emphasize, however, that body forces due to density variations may, on occasion, play a significant role even when device dimensions are relatively small. See, for example, Qian *et al*. (2006).

The electrolyte satisfies the continuity equation:

$$\nabla \cdot \mathbf{u} = 0 . \tag{11}$$

Equations (1-11) constitute the standard model.

In the model presented above, we neglected the induced magnetic field. This is justified since, in all our applications, the magnetic Reynolds number $\mathrm{Re}_m = \frac{\overline{u}H}{\upsilon} << 1$. In the above, $\overline{u}$ is the average flow velocity; H is a length scale associated with the flow; and $\upsilon = \left(\varsigma_0 \sigma_{ionic}\right)^{-1}$ is the "magnetic diffusivity". For example, when $\overline{u} = 1mm/s$, $H = 1mm$ and $\sigma_0 = 1.29 ohm^{-1}m^{-1}$ (0.1M KCl at $25^o C$), $\mathrm{Re}_m \sim 10^{-12}$ and the magnetic induction can be safely neglected. This approximation is valid even in the case of liquid metals. For example, in the case of mercury (conductivity of $10^6 ohm^{-1}m^{-1}$), $\mathrm{Re}_m \sim 10^{-6}$. Thus, in what follows, we assume that the external, imposed magnetic field is unperturbed by the flow.

When the applied magnetic field is uniform ($\mathbf{b} = |\mathbf{b}|\mathbf{e}_z$) and the bulk of the electrolyte solution satisfies the electro-neutrality condition, both $\mathbf{f}_{\nabla B}$ and $\mathbf{f}_E$ vanish, leaving the Lorentz force as the only body force. The dimensionless Navier-Stokes equation becomes:

$$\mathrm{Re}\left(\frac{\partial \hat{\mathbf{u}}}{\partial \hat{t}} + \hat{\mathbf{u}} \cdot \hat{\nabla}\hat{\mathbf{u}}\right) = -\hat{\nabla}\hat{p} + \hat{\nabla}^2\hat{\mathbf{u}} - \mathrm{K}\sum_{i=1}^{l} z_i \hat{D}_{\mathrm{i}} \left(\hat{\nabla}\hat{c}_i + z_i \hat{c}_i \hat{\nabla}\hat{\phi}\right) \times \hat{\mathbf{b}} + \mathrm{Ha}^2 (\hat{\mathbf{u}} \times \hat{\mathbf{b}}) \times \hat{\mathbf{b}} . \tag{12}$$

In the above, $Ha = H|\mathbf{b}|\sqrt{\frac{\sigma_{ionic}}{\mu}}$ is the Hartmann number. The velocity, length, time, concentration, potential, magnetic field, pressure and diffusion coefficients are, respectively, scaled with $u_0 = \frac{F^2 H |\mathbf{b}| D_0 \overline{c}_q \Delta V_{ext}}{\mu RT}$, the conduit's height H, $\frac{u_0}{H}$, the average concentration

$\overline{c}_q$, $\frac{RT}{F}$, $|\mathbf{b}|$, $\frac{\mu u_0}{H}$, and $D_0 = \sum_{i=1}^{l} \frac{1}{|z_i|} \Big/ \sum_{i=1}^{l} \frac{1}{D_i}$. $\mathrm{Re} = \frac{\rho u_0 L}{\mu}$ is the Reynolds number. $\mathrm{K} = \frac{F|\mathbf{b}| D_0 \overline{c}_q H}{\mu u_0}$ is the ratio between the Lorentz force and the viscous force.

The dimensionless current $\hat{\mathbf{j}} = \frac{\mathbf{j}}{j_0} = -\mathrm{K} \sum_{i=1}^{l} z_i \hat{D}_i \left(\nabla \hat{c}_i + z_i \hat{c}_i \nabla \hat{\phi} \right) + \mathrm{Ha}^2 (\hat{\mathbf{u}} \times \hat{\mathbf{b}})$, where $j_0 = \frac{\mu u_0}{H^2 |\mathbf{b}|}$. ΔV_{ext} is the externally applied potential difference. Overhats denote dimensionless quantities and overbars denote domain averages. When the Hartmann number is small, the induction current term in equation (12) can be neglected. This is generally the case in microfluidic systems operating with electrolyte solutions. For example, when $H = 1mm$, $|\mathbf{b}| = 0.4T$, $\mu = 10^{-3} Pa \cdot s$ and $\sigma_{ionic} \sim 1 ohm^{-1} m^{-1}$ (0.1M KCl at $25^o C$), the Hartmann number $Ha \sim 10^{-2}$. In contrast, in the case of liquid metals such as mercury (conductivity $10^6 ohm^{-1} m^{-1}$), $Ha \sim 10$ and the induction current term in equation (12) must be taken into account.

Equation (4) suggests that there is no accumulation of charge in the bulk of the solution. Therefore, the current flux is solenoidal (divergence free).

$$\nabla \cdot \mathbf{j} = 0 . \tag{13}$$

Applying equation (13) to equation (5) and neglecting the induction term, we obtain the equation for the electric potential in the bulk of the solution:

$$\nabla \cdot \left(\sigma_{ionic} \nabla \phi \right) + F \sum_{i=1}^{l} z_i \nabla \cdot \left(D_i \nabla c_i \right) = 0 . \tag{14}$$

Witness that equation (14) reduces to Ohm's law only when one can neglect the term $F \sum_{i=1}^{l} z_i \nabla \cdot \left(D_i \nabla c_i \right)$. This would be the case when all the ionic species have similar diffusivities or when the concentration distributions are nearly uniform. The flow field affects equation (14) indirectly through its effect on the concentration field (equation 2).

When reversible reactions of the type $Ox + ne^- \Leftrightarrow Red$ take place at the electrodes' surfaces, the species' fluxes at the electrodes' surfaces are given by the Butler-Volmer (**BV**) equation [1]:

$$\mathbf{n}\cdot\mathbf{N}_{Red} = \frac{j_e}{F}\left[\frac{c_{Ox}}{\overline{c}_{Ox}}e^{(-\alpha nF/RT)\eta} - \frac{c_{Red}}{\overline{c}_{Red}}e^{[(1-\alpha)nF/RT]\eta}\right] = -\mathbf{n}\cdot\mathbf{N}_{Ox}\ , \tag{15}$$

where j_e is the exchange current flux, α is the charge transfer coefficient for the cathodic reaction, n is the number of electrons exchanged in the reaction, $\eta = \phi - V_{ext}$ is the overpotential, and c_{Ox} and c_{Red} are, respectively, the concentrations of the oxidized and reduced species at the electrodes' surfaces. $\mathbf{n}$ is a unit vector normal to the electrode's surface directed away from the fluid. When concurrent, multiple reactions take place at the electrodes' surfaces, a separate BV equation is needed for each reacting pair. All solid surfaces, other than the electrodes, are impermeable.

The boundary conditions associated with the momentum equation are no slip at all solid surfaces. In the problems considered here, we specify periodic conditions for the flow velocities at the inlet and outlet.

Electrical neutrality exists in the bulk of the solution, but not next to solid surfaces. Typically a surface in contact with an aqueous solution acquires a net charge, which attracts counterions to form a thin (a few nanometers in thickness) electrical double layer consisting mostly of counterions. The electric field's component tangent to the surface propels the ions in the electric double layer and gives rise to electroosmotic flow. When the device's length scale is much greater than the thickness of the EDL, the flow in the EDL is approximated by the Smoluchowski slip velocity (Probstein 1994):

$$u_{//} = -\varepsilon_s \zeta E_{//} / \mu\ , \tag{16}$$

where the zeta potential ζ is the potential difference across the EDL and E is the electric field. The subscript // denotes the vector component tangent to the solid/liquid interface.

3 On the Existence of MHD Potential in Some Special Cases

Many microfluidic systems are planar (i.e., parallel to the *x*-*y* plane, **Fig. 1**). Since the conduits' depths (W in the $z-$direction) are relatively small, the magnetic field is nearly uniform and parallel to the $z-$direction, i.e., $\mathbf{b}=|\mathbf{b}|\mathbf{e}_z$, where $\mathbf{e}_z$ is a unit vector in the $z-$direction. Often, the electrodes and embedded features, such as pillars, are parallel to the $z-$axis and extend the entire conduit's depth. See Fig. 1 for an example. Under these conditions, the current flux and the Lorentz force can be expressed, respectively, with vectors $\mathbf{j}(x,y)=j_x(x,y)\mathbf{e}_x+j_y(x,y)\mathbf{e}_y$ and $\mathbf{f}_L(x,y)=|\mathbf{b}|\left(j_y(x,y)\mathbf{e}_x-j_x(x,y)\mathbf{e}_y\right)$ that are independent of the $z-$coordinate. Although we used in the above Cartesian coordinates, the same holds true for any cylindrical coordinate system (Moon and Spencer 1988). Given that the electric current flux is solenoidal and $\mathbf{b}$ is constant, the Lorentz force $\mathbf{f}_L$ is irrotational (curl-free). To see this, consider

$$\nabla\times\mathbf{f}_L=\nabla\times\mathbf{j}\times\mathbf{b}=\mathbf{j}\left(\nabla\cdot\mathbf{b}\right)-\mathbf{b}\left(\nabla\cdot\mathbf{j}\right)+\left(\mathbf{b}\cdot\nabla\right)\mathbf{j}-\left(\mathbf{j}\cdot\nabla\right)\mathbf{b}=0. \tag{17}$$

The first and last terms on the RHS of equation (17) vanish because $\mathbf{b}$ is a constant. The second term vanishes because the electric current flux is solenoidal ($\nabla\cdot\mathbf{j}=0$). The third term vanishes because, in our particular case, $\mathbf{b}$ and $\mathbf{j}$ are orthogonal and $\mathbf{j}$ doesn't vary in the direction of $\mathbf{b}$ (the z-direction). In other words, the Lorentz force is a conserving vector field, and one can define the "Lorentz potential" Ξ such that

$$\mathbf{f}_L=-\nabla\Xi. \tag{18}$$

We emphasize that the Lorentz "potential" exists only in the special circumstances outlined above. Although these circumstances occur frequently in microfluidic systems, they *do not* apply to MHD flows in general. Unless the outlined special circumstances are satisfied, the Lorentz force is *not* curl-free.

Since in microfluidic systems the Reynolds number is typically small, one can neglect inertial effects in equation (12). In the absence of magnetophoretic and electrostatic forces, the dimensionless Stokes equation can be rewritten as

$$-\hat{\nabla}(\hat{p}+\hat{\Xi})+\hat{\nabla}^2\hat{\mathbf{u}}=0 \tag{19}$$

so that the pressure can be modified to include the Lorentz "potential," $\hat{\Xi}=\frac{\Xi}{j_0|\mathbf{b}|}$. On account of the continuity equation, we also have

$$\hat{\nabla}^2(\hat{p}+\hat{\Xi})=0\,. \tag{20}$$

Hence, when the boundary conditions are equivalent, the MHD flow patterns are similar to pressure driven flow patterns.

In this section, we have shown that under special circumstances, which often occur in microfluidic systems, the MHD flow is equivalent to pressure-driven flow. Consequently, one can utilize the wealth of data available in the literature for pressure-driven flows to infer MHD flow patterns, as we demonstrate through a few examples in the following sections.

4 MHD Flow in a Conduit with a Uniform Cross-Section (MHD Pump)

Consider a straight conduit with rectangular cross-section of width W and height H (Fig. 1b without the pillar). The opposing walls of the conduit ($y=\pm\frac{H}{2}$) are plated with electrodes along the conduit's entire length L. An external potential difference ΔV_{ext} is imposed across the electrodes. It is well-known that the classical expression for fully-developed, pressure driven flow (White 2006) can be used to describe the velocity profile of low Hartman number, MHD flow in a conduit with a uniform, rectangular cross-section. Indeed, this is a special consequence of the derivation presented in section 3. The flow rate is (Bau et al. 2003):

$$Q=\frac{1}{R_H}\left(-\frac{dp}{dx}+j_y|\mathbf{b}|\right). \tag{21}$$

where $R_H = \dfrac{12\mu}{\chi W H^3}$ is the hydraulic resistance of the pump and $\chi = 1 - \dfrac{192H}{\pi^5 W}\sum_{n=0}^{\infty}\dfrac{1}{(1+2n)^5}\tanh\dfrac{(1+2n)\pi W}{2H}$. Witness that the sum in χ converges rapidly and, in many cases, just the first two terms in the series provide an adequate approximation. In the absence of an external pressure gradient, the average velocity is proportional to the $y-$ component of the current flux j_y. The stall pressure is $\Delta p_{stall} = |\mathbf{b}|\, I/W = |\mathbf{b}|\, j_y L$, where $I = j_y LW$ is the total current transmitted between the electrodes. Equation (21) can be rewritten in a slightly different form

$$Q = Q_{\max}\left(1 - \frac{\Delta p_b}{\Delta p_{stall}}\right). \tag{22}$$

In the above, $Q_{\max}$ is the flow rate in the absence of adverse (back) pressure and Δp_b is the back pressure.

4.1 Current-Potential Relationship in the MHD Pump

In contrast to the case of liquid metals, in the case of electrolyte solutions, the current density is not a linear function of the potential difference across the electrodes. Furthermore, as the potential difference across the electrodes increases, the current eventually reaches a limiting value.

To illustrate the complex current-potential dependence, we consider the reversible reaction $A^{z_1+} + (z_1 - z_2)e^- \Leftrightarrow B^{z_2+}$ of the RedOx species A^{z_1+}, B^{z_2+}, and C^{z_3-}. A specific example consists of the solution Fe^{3+}, Fe^{2+}, and Cl^- with the reducing reaction $Fe^{3+} + e^- \rightarrow Fe^{2+}$ at the cathode and the oxidizing reaction $Fe^{3+} \rightarrow Fe^{2+} + e^-$ at the anode. The steady state, dimensionless equations (1) and (2) reduce to:

$$\begin{aligned}
&\frac{d\hat{c}_1}{d\hat{y}} + z_1\hat{c}_1\frac{d\hat{\phi}}{dy} = -\frac{\hat{j}_{\hat{y}}}{z_1 - z_2} \\
&\frac{d\hat{c}_2}{d\hat{y}} + z_2\hat{c}_2\frac{d\hat{\phi}}{dy} = \frac{D_1}{D_2}\cdot\frac{\hat{j}_{\hat{y}}}{z_1 - z_2} \\
&\frac{d\hat{c}_3}{d\hat{y}} - z_3\hat{c}_3\frac{d\hat{\phi}}{dy} = 0
\end{aligned} \tag{23}$$

In the above, the concentrations are normalized with $\overline{c}_3$ and the current's density with $D_1 F\overline{c}_3 / H$. In general, equations like (23) must be solved numerically. Here, we consider a special case which allows us to obtain a relatively simple expression for the current-potential relationship.

Let $\overline{c}_1 = g\overline{c}_3$. When $z_1 = 3,\ z_2 = 2$, and $z_3 = 1$ (as in the case of ferri/ferro-chloride), and $D_1 / D_2 = 3/4$, one obtains (Grigin 1993) $\left(\hat{c}_1 + \hat{c}_2\right)\left(3c_1 + 2c_2\right) = m$, where m is an integration constant. Using mass conservation, one can determine m as a function of $\hat{j}_{\hat{y}}$ for any g. In the absence of current ($\hat{j}_{\hat{y}} = 0$), $m = (1-g)/2$. It turns out that m is nearly independent of $\hat{j}_{\hat{y}}$. Using the Butler-Volmer boundary conditions (15), we obtain an implicit relation between the current and the electrodes' potential difference (Qin and Bau, 2009) (**Fig. 2)**. The hollow circles, crosses, and solid line correspond, respectively, to the exact solution (which does not assume fixed m), an analytic solution that assumes $m \sim (1-g)/2$, and a finite element solution of the NP equations. Witness that as the potential difference between the electrodes increases, the current flux initially increases slowly, then nearly linearly, and, eventually, it saturates at higher values of the potential difference. When $D_1 = 10^{-9} m^2/s$, $\overline{c}_3 = 1M$ and $H = 1mm$, the maximum (limiting) current is $j_{y,\lim} = 45.3A/m^2$ (Fig. 2). For a conduit with width $W = 1mm$, flow viscosity $\mu = 10^{-3} Pa\cdot s$, and magnetic field $|\mathbf{b}| = 0.4T$, the predicted average MHD velocity is ~0.6 mm/s.

One take-away message is that, generally, in electrolyte solutions, the current is a nonlinear function of the potential difference across the electrodes. A linear relationship between the current and the potential difference can be assumed only for a limited range of operating conditions. The second observation is the existence of a limiting current. In other

words, the amount of electric current that can be transmitted through the electrolyte solution does not increase monotonically with increasing potential difference due to mass transfer limitations (diffusion limited reaction). Although, in practice, further increases in the potential difference across the electrodes may increase the current flux, this increase will typically be due to other (usually undesirable) electrochemical interactions at the electrode surfaces such as the electrolysis of water. In a closed system, the electrolysis of water will cause the formation of a gas blanket along the electrodes' surfaces that will greatly reduce the amount of current transmitted in the solution.

4.2 The Average Velocity and Efficiency of the MHD Pump

Kabbani *et al.* (2007) and Ho (2007) investigated the flow rate and the average velocity in the MHD pump as functions of the conduit's dimensions when the current injection is controlled. Since, in most applications, one controls the electrodes' potentials rather than the current, we briefly comment here on the situation when the potential difference between the electrodes is controlled. The current flux j_y is inversely proportional to the distance between the electrodes H. The flow rate in the absence of external back pressure: $Q = \frac{|\mathbf{b}| D_1 F \overline{c}_3 \hat{j}_{\hat{y}}}{12\mu} \chi H^2 W$ and the fluid's average velocity is

$$\overline{u} = \frac{|\mathbf{b}| D_1 F \overline{c}_3 \hat{j}_{\hat{y}}}{12\mu} \chi H \,. \tag{24}$$

The above expression is valid when the entire conduit's length is decorated with active electrodes.

Fig. 3 depicts the average flow velocity as a function of the conduit's height and width when $|\mathbf{b}| = 0.4T$, $D_1 = D_3 = 10^{-9} m^2/s$, $\overline{c}_1 = \overline{c}_2 = 0.2M$, $\overline{c}_3 = 1M$, $\Delta \hat{V}_{ext} = 32$, $\hat{j}_{\hat{y}} = 0.42$, and $\mu = 10^{-3} Pa \cdot s$. We assume that W is sufficiently small compared to the size of the source of the magnetic field so that the magnetic field is nearly uniform inside the conduit.

At a fixed conduit width, as the height H increases, $\overline{u}$ first increases, attains a maximum at $H \sim W$, and then decreases. This behavior results from the drag force attaining a minimum in a square ($H = W$) cross-section while the total Lorentz driving force is nearly

independent of the conduit's height. The latter is true because the current's density is inversely proportional to the distance between the electrodes ($j_y \propto 1/H$) and the Lorentz force is the product of the magnetic field, the current's density and the fluid's volume. Thus, the total force is independent of the distance between the electrodes.

In the limit of $H >> W$, we approach the case of flow between two, infinite parallel plates, and the resistance imposed by the top ($y = H/2$) and bottom ($y = -H/2$) walls (the electrodes) can be neglected. Under this circumstance, along most of the conduit's cross-section, the velocity profile is parabolic in the *z*-direction and independent of *y*. The drag force is proportional to H/W and the Lorentz force is proportional to W . Thus, the average velocity is proportional to W^2/H . Witness the parabolic increase in the average velocity with W and the inverse proportionality to H in Fig. 3 when H is large and W is small. As W increases, the drag induced by the surfaces $y = \pm H/2$ starts to play a role and the rate of increase of the average velocity with W declines. When W is large, the average velocity is independent of W .

The MHD–induced velocities are relatively small. For example, in the case of the RedOx pair $FeCl_3/FeCl_2$ ($D_1 = 6.04\times10^{-10} m^2/s$, $D_2 = 7.19\times10^{-10} m^2/s$, $D_3 = 2.03\times10^{-9} m^2/s$, and exchange current density $j_e = 10^{-6} A/m^2$, Qian and Bau, 2005) at maximum solute concentrations $c_1 = 1.54M, c_2 = 2.05M$, and $c_3 = 8.73M$, the limiting current density $j = 208.1A/m^2$ and the average flow velocity $\bar{u} = 2.9mm/s$ when $W = H = 1mm$ and $|\mathbf{b}| = 0.4T$. More appreciable velocities can be attained with higher conductivity electrolytes.

We define the MHD pump's efficiency as the power needed to drive the flow, which includes both the power needed to overcome the drag (internal resistance) in the pump and the power invested to overcome the adverse (back) pressure, normalized with the electrical power consumed.

$$eff = \frac{\Delta p_{stall} Q}{\Delta V_{ext} I}. \tag{25}$$

Our definition of the efficiency differs from that of Laser and Santiago (2004) and Ramos (2007), who treated the power needed to overcome the drag as internal pump loss and did not include it in the numerator of equation (25). Occasionally, MHD microfluidic systems and networks operate without any external backpressure. Given that the entire length of conduits in microfludic devices may be equipped with electrodes and backpressure may be absent, it is appropriate to count the work carried out against the internal drag as part of the pump's output. In view of equation (22), the maximum efficiency is attained in the absence of backpressure ($\Delta p_b = 0$), i.e., $eff_{\max} = \dfrac{\Delta p_{stall} Q_{\max}}{\Delta V_{ext} I}$. Fig. 4 depicts schematically the flow rate in the MHD pump (Q) as a function of the backpressure (Δp_b). The large rectangle ($\Delta p_{stall} Q_{\max}$) represents the maximum work delivered by the MHD pump. This is the work interaction used in our expression for the maximum pump efficiency. The smaller rectangle $\dfrac{1}{4}\Delta p_{stall} Q_{\max}$ is the work interaction used in Laser and Santiago's (2004) definition of the maximum efficiency. The efficiency given in equation (25) is four times larger than the value reported in Laser and Santiago (2004).

Upon substituting the expressions for the flow rate and the pressure drop, we can rewrite the efficiency (in the absence of backpressure) as:

$$eff = \frac{|\mathbf{b}|^2 D_1 F^2 \overline{c}_3}{12 \mu R T} \cdot \frac{\hat{j}_{\hat{y}}}{\Delta \hat{V}_{ext}} \cdot \chi H^2 . \qquad (26)$$

Equation (26) suggests that for a given conduit geometry, the efficiency depends on the ratio $\hat{j}_{\hat{y}} / \Delta \hat{V}_{ext}$. **Fig. 5** depicts the ratio $\hat{j}_{\hat{y}} / \Delta \hat{V}_{ext}$ as a function of $\Delta \hat{V}_{ext}$. Witness that this ratio attains its maximum when $\Delta \hat{V}_{ext} = 32$ and $\hat{j}_{\hat{y}} = 0.42$.

Fig. 6 depicts the maximum efficiency as a function of the conduit's height and width when $|\mathbf{b}| = 0.4T$, $D_1 = D_3 = 10^{-9} m^2/s$, $D_2 = 4/3 \times 10^{-9} m^2/s$, $\overline{c}_1 = \overline{c}_2 = 0.2M$, $\overline{c}_3 = 1M$, $\Delta \hat{V}_{ext} = 32$, $\hat{j}_{\hat{y}} = 0.42$, and $\mu = 10^{-3} Pa \cdot s$. **Fig. 6** suggests that MHD pumps operating with electrolyte solutions have extremely low efficiency. The efficiency of the pump can be somewhat increased by using higher electrolyte molar concentrations to increase the electric conductivity of the solution. Almost all the energy dissipated in the MHD pump is

converted into heat. Nevertheless, the temperature increase of the electrolyte solution is relatively small. This is because of the relatively small dimensions of the conduits encountered in microfluidics, which facilitate highly efficient heat interaction with the ambient.

To estimate the temperature increase that one may expect in MHD flow, we consider the particular example of a conduit with a $1mm \times 1mm$ cross-section embedded in a $2mm$ thick polycarbonate (pc) sheet. **Fig. 7** depicts the cross-section of the conduit and the substrate in which the conduit is embedded. The heat transfer coefficient at the surface of the plastic is assumed to be $h \sim 5W/m^2 \cdot K$, which is at the low end of heat transfer coefficients corresponding to natural convection in air. When the applied potential is $\Delta V_{ext} = 40RT/F$, the current's density is $j_y = 45.3A/m^2$, and the heat dissipation per unit volume is $46.5kW/m^3$, the maximum temperature in the conduit is $\sim 0.5K$ above the ambient temperature. The thermal properties used are: $\rho_{fluid} = 1000kg/m^3$, $C_{p,fluid} = 1.2kJ/kg \cdot K$, $k_{fluid} = 0.21W/m \cdot K$, $\rho_{pc} = 1300kg/m^3$, $C_{p,pc} = 4.18kJ/kg \cdot K$ and $k_{pc} = 0.6W/m \cdot K$

5 MHD Flow in a Conduit Patterned with a Pillar Array

In this section, we consider a uniform, long conduit patterned with a pillar array. **Fig. 1** depicts one unit cell of depth W. The pillar diameter is d and the pillar's center is at the conduit's mid-width (**Fig. 1a**). We focus on a two-dimensional case ($W >> H, L$) in the absence of an external pressure gradient. We first consider the case when the current supplied to the unit cell is controlled (known) and one wishes to determine the flow pattern and the flow rate. To this end, we take advantage of results available in the literature for pressure-driven flows.

Integrating equation (19) over the volume of interest, we have, in the absence of external pressure differences:

$$\begin{aligned} \iint_{S} \boldsymbol{\tau}_w \cdot d\mathbf{S} &= \mathbf{F}_{drag,cylinder} + \mathbf{F}_{drag,walls} \\ &= \iiint_{V} |\mathbf{b}|\, j_y(x,y)\mathbf{e}_x dV \\ &= |\mathbf{b}|\, IL \cdot \mathbf{e}_x \end{aligned} \tag{27}$$

where $\boldsymbol{\tau}_w$ is the stress tensor at the conduit's walls and the pillar's surface. The stress includes both pressure and viscous contributions. $\mathbf{S}$ is the surface enclosing the volume V. The drag coefficient $\lambda = \dfrac{F_{drag}}{\mu \bar{u} W}$. In the Stokes regime, the drag coefficients associated with both the cylinder and the conduit wall depend only on the geometry (Faxen 1946). Once the total current injection I is known, one can use the drag coefficient and the equivalency between pressure driven flow and MHD flow to compute the average velocity

$$\bar{u} = \frac{|\mathbf{b}|\, IL}{\mu(\lambda_{cylinder} + \lambda_{walls})W}. \tag{28}$$

The drag coefficient of a single circular pillar placed midway between two long, flat plates as a function of the ratio of the pillar's diameter and the distance between the plates is available in Harrison (1924), Faxen (1946) and Ben Richou *et al.* (2004). There's also a wealth of data for drag coefficients of pressure driven flow around pillar arrays. For example, Sangani and Acrivos (1982) provide drag coefficients of square and hexagonal pillar arrays.

For conciseness, we consider here in detail only a single row of uniformly spaced pillars confined between two parallel electrodes (Fig. 1). We carried out one set of finite element simulations in which we specified the pressure drop across the length of the conduit, obtained the flow field, and determined the drag coefficient. In another set of simulations, we applied a potential difference across the electrode, specified the electrolyte's properties and solved the Nernst Planck equations with electro-neutrality (section 2) with finite elements to obtain the current distribution, the Lorentz body force, and the corresponding drag coefficients. In both cases, periodic velocity boundary conditions were specified at the flow inlet ($x = -L/2$) and exit ($x = L/2$). **Fig. 8** depicts the drag coefficient associated with the pillar and the conduit's walls as functions of the pillar's diameter normalized with the conduit's width (H). The solid lines and symbols correspond, respectively, to the drag coefficients obtained with the pressure-driven flow simulations and the MHD simulations.

The dashed line and hollow circles correspond to the pillar's drag coefficient, and the solid line and hollow squares correspond to the drag coefficient associated with the conduit's walls. The unit cell dimensions are $H = L = 1mm$. The electrolyte solution consisted of three ionic species with $D_i = (1, 4/3, 1) \times 10^{-9} m^2/s$, $\overline{c_i} = (0.2, 0.2, 1)M$, and $z_i = (3, 2, -1)$. In the Buttler-Volmer equation, we specified $\alpha = 0.5$ and $j_e = 10^{-6} A/m^2$. Given the theory presented in section 3 on the equivalence between MHD flow and pressure-driven flow, it is not surprising that the drag coefficients associated with these two flows are identical.

When the total current is given, it is a simple matter to take advantage of the data available in the literature for pressure-driven flows to determine the MHD velocity profile and the flow rate. The same method can be applied to situations when the fluid is subjected to both Lorentz body force and pressure gradients (either assisting or adverse). Since the momentum equation is linear at low Reynolds numbers, one can simply superpose MHD and pressure-driven flows.

Matters get more complicated when the potential difference between the electrodes is the control input rather than the electric current. In this case, to obtain the concentration distribution, one requires knowledge of the flow field and to obtain the flow field, one needs to know the current, which, in turn, depends on the concentration distribution. Since the various fields are coupled nonlinearly, one cannot take advantage of superposition. When the effects of advection on the concentration distribution cannot be neglected, the data available in the literature for pressure driven flow can only be used to verify the MHD computations.

Next, we consider a case when the electrode potential difference is controlled and the current is not apriori known. To obtain the current distribution, we solve the Nernst-Planck equations with Buttler-Volmer boundary conditions together with the Navier-Stokes equations (section 2). **Fig. 9** depicts the total, dimensionless current in the unit cell as a function of d/H when the effects of advection on the concentration distribution are neglected (zero Peclet number, solid line) and when the effect of the flow on the concentration distribution (dashed line with hollow squares) is accounted for. **Fig. 9a** and **9b** correspond, respectively, to a dimensionless potential difference between the electrodes of 25 and 40. Clearly advection significantly affects the current both quantitatively and qualitatively. When $d/H = 0.44$ and $\Delta\hat{V}_{ext} = 25$, neglecting advection leads to a current

underestimate of ~25% (Fig. 9a). When $\Delta\hat{V}_{ext} = 40$, neglecting advection leads to up to a 45% underestimate in the current (Fig. 9b). As the potential difference across the electrodes $\Delta\hat{V}_{ext}$ increases, the magnitude of the velocity increases, advection effects become more important, and the error resulting from neglecting advection increases.

In the absence of advection (solid lines in Fig. 8), as the pillar diameter increases, the current decreases monotonically. This is intuitively expected. As the pillar diameter increases, the area available to current flow decreases and one would expect the current to decrease. Counter to intuition, however, when convection is accounted for (dashed lines in Fig. 8), as the pillar diameter increases from zero, the limiting current initially increases, attains a maximum, and then decreases.

A similar trend is evident in **Fig. 10**. The figure depicts the average dimensionless current flux in the *y*-direction as a function of the potential difference between the electrodes $\Delta\hat{V}_{ext}$ when $d/H = 0$, 0.036, 0.11, 0.16, 0.25, 0.36, 0.71 and 0.8. The electrolyte solution is the same as in **Fig. 9**. As the potential difference $\Delta\hat{V}_{ext}$ increases, the current initially increases slowly, then nearly linearly, and eventually reaches an asymptotic, limiting value $\hat{j}_{\hat{y},lim}$. Witness that the currents associated with $0 < d/H < 0.36$ are higher than the one associated with $d/H = 0$.

What then is the mechanism by which the pillar presence enhances the current flow in certain circumstances? One possible explanation is, that in the presence of the pillar, the magnitude of the velocity $u_x(0, y)$ in the region above and beneath the pillar ($d/2 < |y| < H/2$) increases above the corresponding value upstream of the pillar. This, in turn, increases the concentration gradients next to the electrodes' surfaces and enhances the diffusion's contribution to the current flow. **Fig. 11a** depicts the concentration field c_1 in the presence of the pillar and the MHD flow when $\Delta\hat{V}_{ext}$ =25 and $d/H = 0.2$. The solid longitudinal lines and the transverse solid lines represent, respectively, concentration contour lines and current flux lines. **Fig. 11b** depicts the concentration field c_1 in the presence of a pillar and in the absence of flow motion. **Fig. 11c** depicts the concentration field c_1 in the absence of the pillar. In the last case, the concentration field is independent of the flow. In

cases (b) and (c), the concentration field is symmetric with respect to the $y=0$ axis while in Fig. 11a, due to transverse velocity components in the vicinity of the pillar, the concentration field is asymmetric with respect to the $y=0$ axis. In other words, in the presence of the pillar, there is a transverse velocity component that contributes to electrolyte advection. To better demonstrate the effect of the pillar on the concentration distribution, Figs. 11d and 11e depict, respectively, $c_1(x,H/2)$ along the surface of the cathode as a function of x and $c_1(0,y)$ as a function of y in the presence of motion (solid lines), in an absence of the pillar (dotted line with hollow circles), and in the presence of the pillar and the absence of motion (dashed line). Witness that in the presence of the pillar and the flow, the concentration of c_1 next to the electrode's surface (in the vicinity of $x=0$, solid line, Fig. 11d) is significantly higher than in the absence of a pillar (dotted line with hollow circles) or in the presence of a pillar without flow (dashed line). The latter case demonstrates clearly that, in the absence of flow, the presence of the pillar adversely affect the current flow. The average current is lower than in the absence of a pillar. In the presence of both a pillar and flow, the concentration next to the electrode's surface is higher than otherwise and, thus, the average current flux is higher. Similarly, Fig. 11e shows that the concentration gradient is highest in the presence of the pillar and MHD flow (solid line) and lowest in the presence of a pillar and an absence of flow (dashed line). In summary, on the one hand, the pillar reduces the cross-sectional area available to the current flow and increases the drag, both adversely affecting the flow rate. On the other had, the pillar indirectly modifies that concentration field, which enhances current flow. These two competing effects lead to an optimal pillar size that maximizes current flow.

The pillar could contribute to current flow in yet another way. The electric double layer surrounding the pillar is rich in ions, which is described macroscopically as surface conduction. The Bikerman - Dukhin number quantifies the ratio of the surface conductivity to the bulk conductivity (Bazant *et al.* 2006, Chu and Bazant 2006). Since MHD devices typically operate with moderate DC potential and thin electric double layers, the double layer remains near equilibrium and the Dukin number is much smaller than 1, leading to negligible surface conductance.

In the range of parameters considered here and consistent with equation (26), the flow rate is linearly proportional to the total current. **Fig. 12** depicts the average flow velocities as functions of the current when $d/H = 0.11$, 0.16, 0.25, 0.36, 0.50 and 0.71. **Fig. 13** depicts the average flow velocity as a function of the pillar size when the dimensionless potential difference between the electrodes is $\Delta\hat{V}_{ext} = 25$. Although the current attains its maximum value at $d/H = 0.4$, the flow rate decreases monotonically as d/H increases from zero. In other words, the presence of the pillar enhances the drag to a greater extent than the propulsive force (which is proportional to the current).

6 Conclusions

We describe the mathematical model for MHD flows of electrolyte solutions in microfluidic systems. In general, the model requires the concurrent solution of the Nernst-Planck equations and the momentum equations. The flow field modifies the concentration field and the concentration field affects the electric current, which, in turn, affects the body force in the momentum equation. MHD has the advantage of providing a convenient means to pump and stir fluids and control fluid flow with electrical signals and without a need for moving mechanical components. Flow can be directed along any desired path in a microfluidic network without a need for any valves. The disadvantage of MHD is that it involves a volumetric force that does not scale favorably as the conduit size decreases. MHD pumps operating with electrolyte solutions also have very low conversion efficiency, as only a very small fraction of the electric power is converted into work. More serious shortcomings include the need to operate with electrolyte solutions that undergo reversible reactions to avoid bubble formation and undesirable electrochemical electrode reactions and the limitation on the maximum amount of current that can be transmitted in the solutions. It seems that MHD are most likely to benefit applications in which conduit sizes range from hundreds of micrometers to millimeters – a range of length scales in which the MHD drive provides significantly higher flow rates than electroosmosis.

We have shown that when the Reynolds number is low, the magnetic field is uniform, and the electric field is orthogonal to the magnetic field, the Lorentz body force is irrotational and one can define a “Lorentz” potential. In other words, the MHD flow is equivalent to

pressure-driven flow, and one can use the large body of data available in the literature for pressure-driven flow to deduce the MHD flow patterns and drag coefficients. The above conditions often prevail in microfluidic systems. We utilized this equivalence in two examples. The first example consisted of a uniform conduit. Here, the equivalence between MHD flow and pressure-driven flow has been known for many years. The second example consisted of a conduit patterned with pillars. This is a somewhat more general case as the electric flux is neither unidirectional nor uniform as in the first example. The equivalence between MHD flow and pressure-driven flow allows us to utilize drag coefficients available in the literature for pressure-driven flow to calculate the MHD flow patterns provided that the total electric current is controlled. The use of the MHD – pressure driven flow equivalence requires caution, however, since the emergence of secondary flows such as may evolve when the fluid goes around a bend (Yi and Bau 2003) or a curve will destroy the analogy between MHD and pressure-driven flows.

When the electric potential difference across the electrodes is the control variable, the equivalence between the pressure-driven and MHD flow cannot be utilized directly and one needs to compute the concentration, current, and flow fields simultaneously by solving the coupled Nernst-Planck and Navier-Stokes equations.

Finally, we computed the electric current, concentration, and flow field in a conduit and demonstrated that an optimal pillar diameter exists that maximizes the current flow. It is plausible that even higher current transmission can be obtained by optimizing the shape of the pillar. However, maximum flow rate still happens in the absence of pillars.

Acknowledgments

The work was supported, in part, by NSF STTR Grant #0822723 to SFC Fluidics and by the Nanotechnology Institute of the Ben Franklin Technology Partners of Southeastern Pennsylvania.

References

Alemany A, and Chopart J., P., 2007, An outline of magnetoelectrochemistry, Magnetohydrodynamics –Historical Evolution and Trends. Springer, pp 391-407

Aguilar ZP, Arumugam P, Fritsch I (2006) Study of magnetohydrodynamic driven flow through LTCC channel with self-contained electrodes. J Electroanal Chem 591: 201 – 209

Arumugam PU, Clark EA, Fritsch I (2005) Use of paired, bonded NdFeB magnets in redox magneto-hydrodynamics. Anal Chem 77: 1167 – 1171

Arumugam PU, Fakunle ES, Anderson EC, Evans SR, King KG. Aguilar ZP, Carter CS, Fritsch I (2006) Characterization and pumping-redox magnetohydrodynamics in a microfluidic channel. J Electrochem Soc 153: E185 – E194

Bao J, Harrison JD (2003a) Fabrication of microchips for running liquid chromatography by magnetohydrodynamic flow. Proc 7th Intl Conference on Miniaturized Chemical Biochemical Analysis Systems, 407 – 410

Bao J, Harrison JD (2003b) Design and Fabrication of Microchannels for Magneto-hydrodynamic Flow. Proc ICMENS, 396 – 399.

Batchelor GK (1967) An Introduction to Fluid Dynamics. Cambridge University Press

Bau HH, Zhu J, Yi M (2001) A minute magneto dydro dynamic (MHD) mixer. Sensor Actuator B 79: 207-215

Bazant MZ, Thornton K, Ajdari A (2004) Diffuse charge dynamics in electrochemical systems. Phys Rev E 70, 021506

Bau HH, Zhu J, Qian S, Xiang Y (2003) Magnetohydrodynamically controlled fluidic network. Sensor Actuator B 88: 205-216

Ben Richou A, Ambari A, Naciri JK (2004) Drag force on a circular cylinder midway between two parallel plates at very low Reynolds numbers-Part 1: Poiseuille flow (numerical). Chem Eng Sci 59: 3215-3222

Boum NGB, Alemany A (1999) Numerical simulations of electrochemical mass transfer in electromagnetically forced channel flow. Electrochim Acta 44: 1749-1760

Chu KT, Bazant MZ (2006) Nonlinear electrochemical relaxation around conductors. Phys Rev E 74(1), 011501

Davidson PA (2001) An Introduction to Magnetohydrodynamics. Cambridge Univ Press, Cambridge, UK. ISBN 0521791499, 0521794870

Eijkel JCT, Dalton C, Hayden CJ, Burt JPH, Manz A (2003) A circular ac magneto-hydrodynamic micropump for chromatographic applications. Sensor Actuator B 92: 215-221

Eijkel JCT, Van den Berg A, Manz A (2004) Cyclic electrophoretic and chromatographic separation methods. Electrophoresis 25, 243 – 252

Faxen H (1946) Forces exerted on a rigid cylinder in a viscous fluid between two parallel fixed planes. Proc Roy Soc Swedish Inst Engrg Res 187(1)

Gleeson JP, West J (2002) Magnetohydrodynamic micromixing. Technical Proceedings of the 2002 International Conference on Modeling and Simulation of Microsystems, 318 – 321

Gleeson JP, Roche OM, West J, Gelb A (2004) Modeling annular micromixers. SIAM J Appl Math 64, 1294 – 1310

Grigin AP (1993) Theory of the direct-current flow in Redox systems with one electron transfer reactions, Russ J Electrochem 29(9), 938-943

Harrison WJ (1924) Transactions of the Cambridge Philosophical Society 23: 71

Ho JE (2007) Characteristic study of MHD pump with channel in rectangular ducts, J Marine Sci Tech 15(4) 315-321

Jang J, Lee SS (2000) Theoretical and experimental study of MHD (Magnetohydrodynamic) micropump. Sensor Actuator A 80, 84 – 89

Kabbani H, Wang A, Luo X, Qian S (2007) Modeling RedOx-based magnetohydrodynamics in three-dimensional microfluidic channels. Phys Fluids 19: 083604

Laser DJ, Santiago JG (2004) A review of micropumps, J Micromech Microeng, 14, R35-64

Lemoff AV, Lee AP (2000) An AC magnetohydrodynamic micropump. Sensor Actuator B 63, 178 – 185

Leventis N, Gao XR (2001) Magnetohydrodynamic electrochemistry in the field of Nd-Fe-B magnets: theory, experiment, and application in self-powered flow delivery systems. Anal Chem 73, 3981 – 3992.

Lioubashevski O, Katz E, Willner I (2004) Magnetic force effects on electrochemical processes: A theoretical hydrodynamic model. J Phys Chem B 108: 5778-5784

Martin AJP (1958) Gas Chromatography, edited by Coates VJ, Noebels HJ, Fagerson IS. Academic Press, New York, pp 237–247

Moon P, Spencer DE (1988) Eleven Coordinate Systems. §1 in Field Theory Handbook, Including Coordinate Systems, Differential Equations, and Their Solutions, 2nd ed. New York: Springer-Verlag, pp. 1-48

Newman J (1991) Electrochemical Systems 2nd ed. Prentice-Hall, Englewood Cliffs, NJ

Nguyen B, Kassegne SK (2008) High-current density DC magenetohydrodynamics micropump with bubble isolation and release system, Microfluid Nanofluid 5:383–393

Probstein RF (1994) Physicochemical Hydrodynamics: An Introduction, John Wiley & Sons Inc., New York

Qian S, Bau HH (2005) Magnetohydrodynamic flow of RedOx electrolyte. Phys Fluids 17: 067105

Qian S, Chen Z, Wang J, Bau HH (2006) Electrochemical reaction with RedOx electrolyte in toroidal conduits in the presence of natural convection, Int J Heat Mass Trans 49 (21-22) 3968-3976

Qian S, Bau HH (2009) Magneto-hydrodynamics based microfluidics. Mech Res Commun 36, 10-21

Qin M, Bau HH (2009) Magneto-Hydrodynamic Flow in Electrolyte Solutions. Comsol Conf 2009.

Ramos A (2007) Chapter 2: Electrohydrodynamic and Magnetohydrodynamic Micropumps, Microfluidic Technologies for Miniaturized Analysis Systems. Springer.

Sangani AS, Acrivos A (1982) Slow flow past periodic arrays of cylinders with application to heat transfer. Int J Multiphase Flow 8(1), 193-206

West J, Karamata B, Lillis B, Gleeson JP, Alderman J, Collins JK, Lane W, Mathewson A, Berney H (2002) Application of magnetohydrodynamic actuation to continuous flow chemistry. Lab Chip 2, 224 – 230

West J, Gleeson JP, Alderman J, Collins JK, Berney H (2003) Structuring laminar flows using annular magnetohydrodynamic actuation. Sensor Actuator B 96, 190 – 199

White FM (2006) Viscous Fluid Flow, 3rd ed. McGraw-Hill, New York

Xiang Y, Bau HH (2003) Complex magnetohydrodynamic low-Reynolds-number flows. Phys Rev E 68, 016312

Yi M, Qian S, Bau HH (2002) A magnetohydrodynamic chaotic stirrer. J Fluid Mech 468, 153 – 177

Yi M and Bau HH (2003) The Kinematics of Bend-Induced Mixing in Micro-Conduits, International Journal of Heat and Fluid Flow, 24, 645-656

Zhong J, Yi M, Bau HH (2002) Magneto hydrodynamic (MHD) pump fabricated with ceramic tapes. Sensor Actuator A 96, 59 – 66

Figure Captions

Fig. 1: A schematic depiction of a segment of a flow conduit patterned with pillars. The image on the left is a top view and the image on the right is cross-section A-A. The red, dotted line denotes periodic boundary conditions

Fig. 2: The dimensionless current flux as a function of the dimensionless electrodes' potential difference calculated by solving the full NP equations with finite elements (solid line), using the approximation $m \sim (1-g)/2$ (hollow circles), and using exact m values (crosses). $\alpha = 0.5$. $g = 0.2$. $\hat{j}_e = 10^{-3}$. The dimensionless, limiting current $\hat{j}_{\hat{y},\lim} = 0.47$. $D_2 / D_1 = 4/3$. $D_1 = D_3$

Fig. 3: The average velocity of MHD flow as a function of the conduit height H and width W (equation 24). $|\mathbf{b}| = 0.4T$, $D_1 = 10^{-9} m^2/s$, $\overline{c}_3 = 1M$, $\hat{j}_{\hat{y}} = 0.42$, and $\mu = 10^{-3} Pa \cdot s$

Fig. 4: The pump flow rate (Q) is depicted as a function of the backpressure (Δp_b). The large and small rectangles represent, respectively, the pump's maximum work output used to calculate the pump's maximum efficiency in our paper and in Laser and Santiago, 2004.

Fig. 5: The ratio of $\hat{j}_{\hat{y}} / \Delta\hat{V}_{ext}$ as a function of $\Delta\hat{V}_{ext}$. The conditions are the same as in Fig. 2

Fig. 6: The maximum MHD pumping efficiency (equation 26) as a function of the conduit's height H and width W . $\Delta\hat{V}_{ext} = 32$ and all the other parameters are the same as in Fig. 3

Fig. 7: Temperature distribution (contours of constant temperature) in and around a MHD conduit embedded in a polycarbonate sheet. The chip size is $8mm \times 2mm$ and the conduit's cross-section is $1mm \times 1mm$

Fig. 8: The drag coefficient at the pillar's surface (dashed line and hollow circles) and at the conduit's surface (solid line and hollow squares) as functions of the pillar's diameter normalized with the conduit's width (H). The lines and symbols correspond, respectively, to pressure-drive flow and the solution of the NP-NS model. For MHD flow, we used $|\mathbf{b}| = 0.4T$, $D_1 = D_3 = 10^{-9} m^2/s$, $D_2 = 4/3 \times 10^{-9} m^2/s$, $z_1 = 3, z_2 = 2, z_3 = -1$, $\overline{c}_1 = \overline{c}_2 = 0.2M$, $\overline{c}_3 = 1M$, $\Delta\hat{V}_{ext} = 25$, $\rho = 10^3 kg/m^3$, $\mu = 10^{-3} Pa \cdot s$, $H = W = 1mm$, $\alpha = 0.5$ and $j_e = 10^{-6} A/m^2$

Fig. 9: The average y-component of the dimensionless current flux as a function of d/H in the absence (solid line) and the presence (dashed line with hollow squares) of MHD flow. The potential difference between the electrodes is $\Delta\hat{V}_{ext} = 25$ (a) and 40 (b). All other conditions are the same as in Fig. 8

Fig. 10: The average dimensionless current flux $\overline{\hat{j}}_{\hat{y}}$ as a function of the applied dimensionless potential difference $\Delta\hat{V}_{ext}$ when $d/H = 0$, 0.036, 0.11, 0.16, 0.25, 0.36, 0.71 and 0.8. All other conditions are the same as in Fig. 8

Fig. 11: (a) The concentration field c_1 in the presence of a cylinder ($d/H = 0.2$) and MHD flow. (b) The concentration field for c_1 in the presence of a cylinder ($d/H = 0.2$) and in the absence of motion. (c) The concentration field c_1 in the absence of a cylinder. The color code and the solid longitudinal lines in (a), (b), and (c) correspond, respectively, to concentration and concentration contours. The transverse solid lines are the current fluxes. The arrows are velocity vectors. (d) The concentration distribution $c_1(x,-H/2)$ along the surface of the cathode as a function of x in the presence of motion (solid line), in the absence of the cylinder (dotted line with hollow circles), and in the presence of the cylinder and an absence of motion (dashed line). (e) The concentration distribution $c_1(0,y)$ as a function of y in the presence of motion (solid line), in the absence of the cylinder (dotted line with hollow circles), and in the presence of the cylinder and an absence of motion (dashed line). $\Delta\hat{V}_{ext} = 25$. All other conditions are the same as in Fig. 8

Fig. 12: The average flow velocity $\overline{u}$ as a function of the average dimensionless current $\overline{\hat{j}}_{\hat{y}}$ when $d/H = 0.11$ (square), 0.16 (circle), 0.25 (upright triangle), 0.36 (cross), 0.50 (downward triangle) and 0.71 (diamond). All other conditions are the same as in Fig. 8

Fig. 13: The average flow velocity $\overline{u}$ as a function of d/H at $\Delta\hat{V}_{ext} = 25$. All other conditions are the same as in Fig. 8. $d/H = 0$ corresponds to an empty, straight conduit (in the absence of pillars).

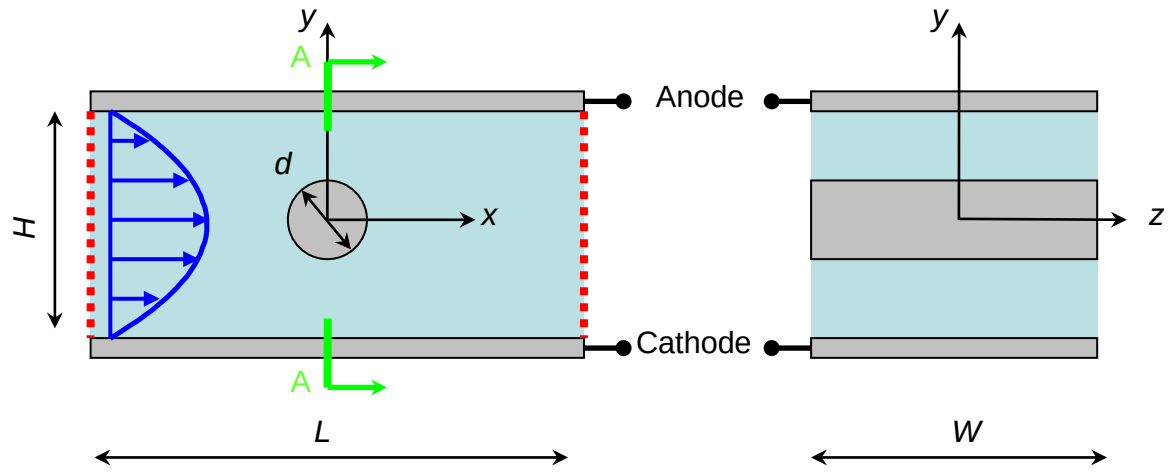

Fig. 1: A schematic depiction of a segment of a flow conduit patterned with pillars. The image on the left is a top view and the image on the right is cross-section A-A. The red, dotted line denotes periodic boundary conditions

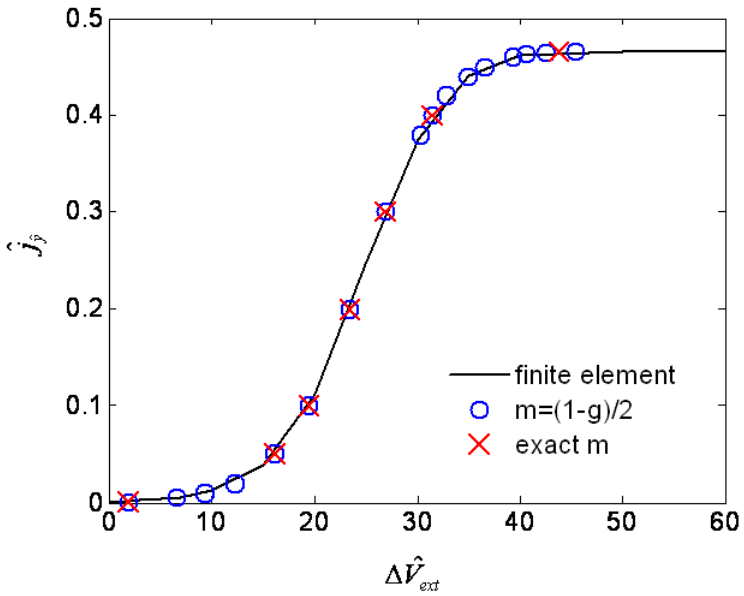

Fig. 2: The dimensionless current flux as a function of the dimensionless electrodes' potential difference calculated by solving the full NP equations with finite elements (solid line), using the approximation $m \sim (1-g)/2$ (hollow circles), and using exact m values (crosses). $\alpha = 0.5$. $g = 0.2$. $\hat{j}_e = 10^{-3}$. The dimensionless, limiting current $\hat{j}_{\hat{y},\lim} = 0.47$. $D_2 / D_1 = 4/3$. $D_1 = D_3$

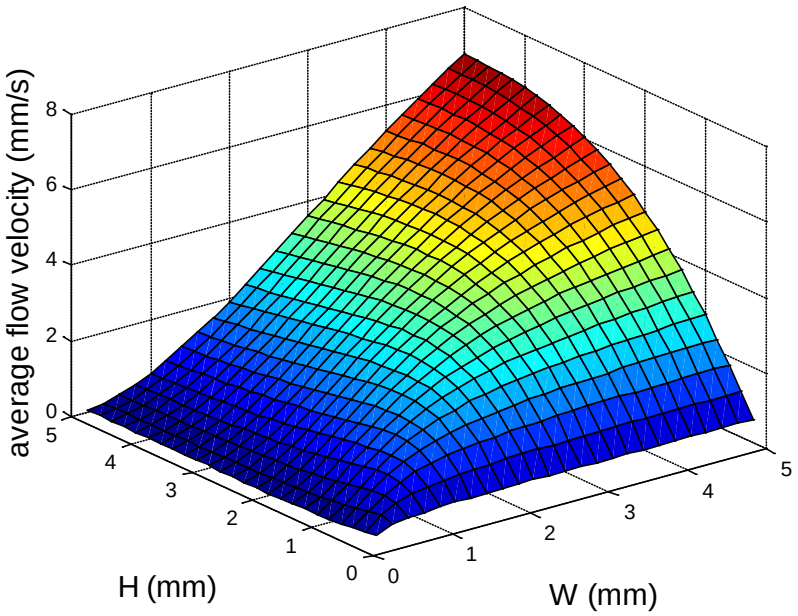

Fig. 3: The average velocity of MHD flow as a function of the conduit height H and width W (equation 24). $|\mathbf{b}| = 0.4T$, $D_1 = 10^{-9} m^2/s$, $\bar{c}_3 = 1M$, $\hat{j}_{\hat{y}} = 0.42$, and $\mu = 10^{-3} Pa \cdot s$

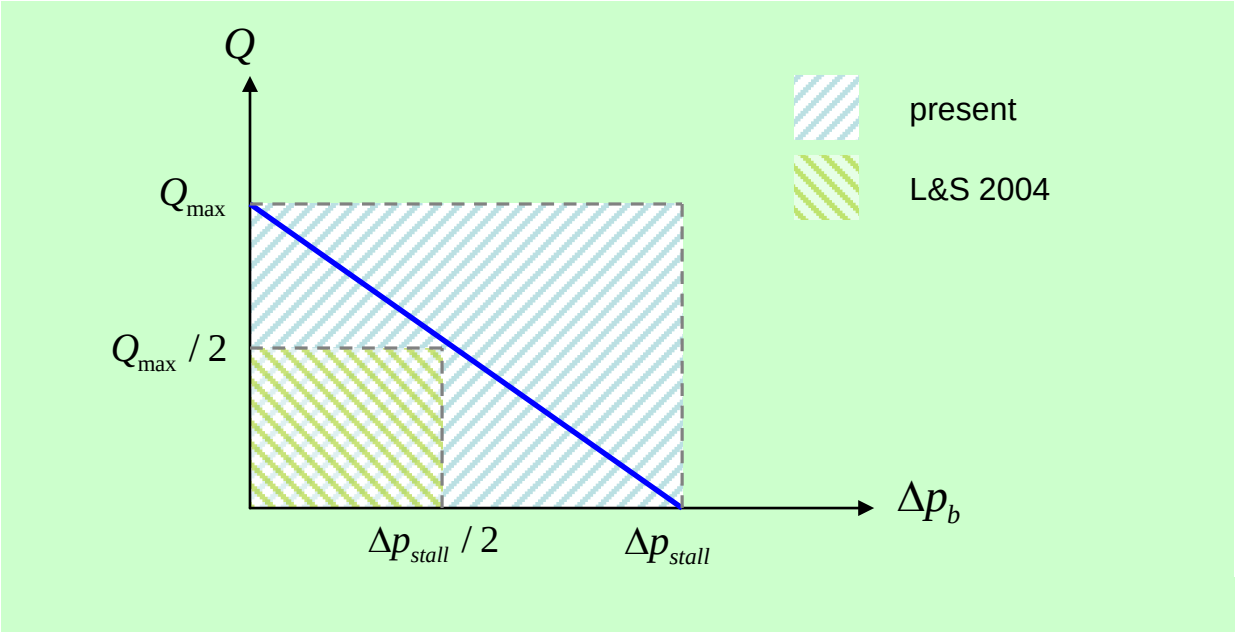

Fig. 4: The pump flow rate (Q) is depicted as a function of the backpressure (Δp_b). The large and small rectangles represent, respectively, the pump's maximum work output used to calculate the pump's maximum efficiency in our paper and in Laser and Santiago, 2004.

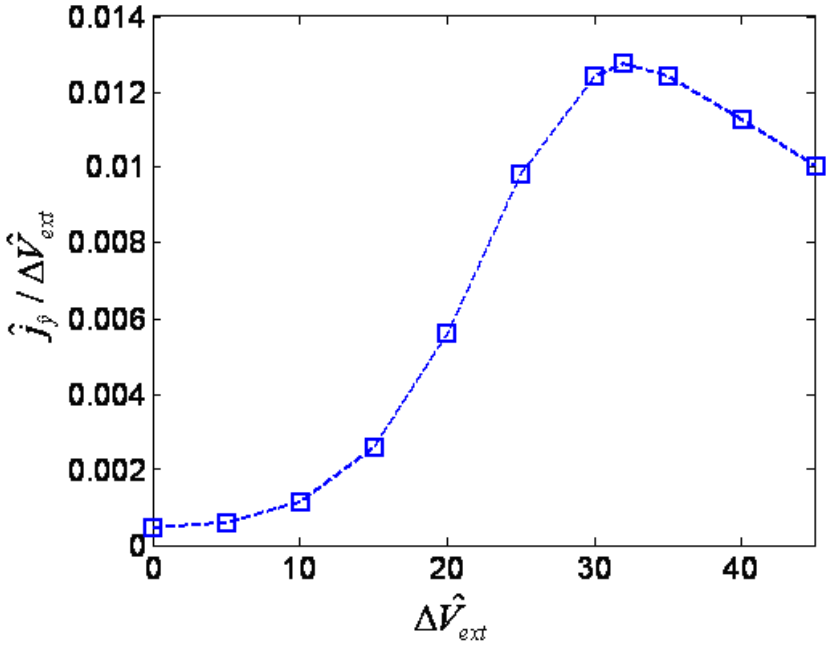

Fig. 5: The ratio of $\hat{j}_{\hat{y}} / \Delta\hat{V}_{ext}$ as a function of $\Delta\hat{V}_{ext}$. The conditions are the same as in Fig. 2

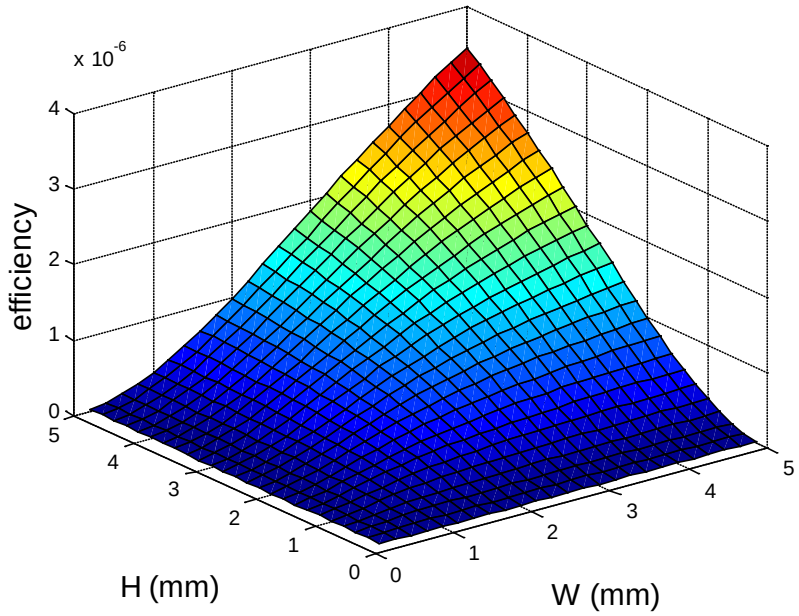

Fig. 6: The maximum MHD pumping efficiency (equation 26) as a function of the conduit's height H and width W. $\Delta\hat{V}_{ext} = 32$ and all the other parameters are the same as in Fig. 3

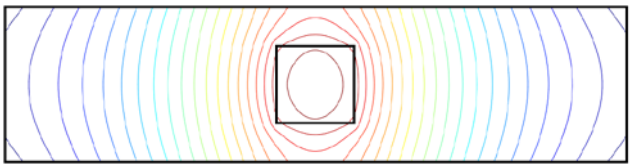

Fig. 7: Temperature distribution (contours of constant temperature) in and around a MHD conduit embedded in a polycarbonate sheet. The chip size is $8mm \times 2mm$ and the conduit's cross-section is $1mm \times 1mm$

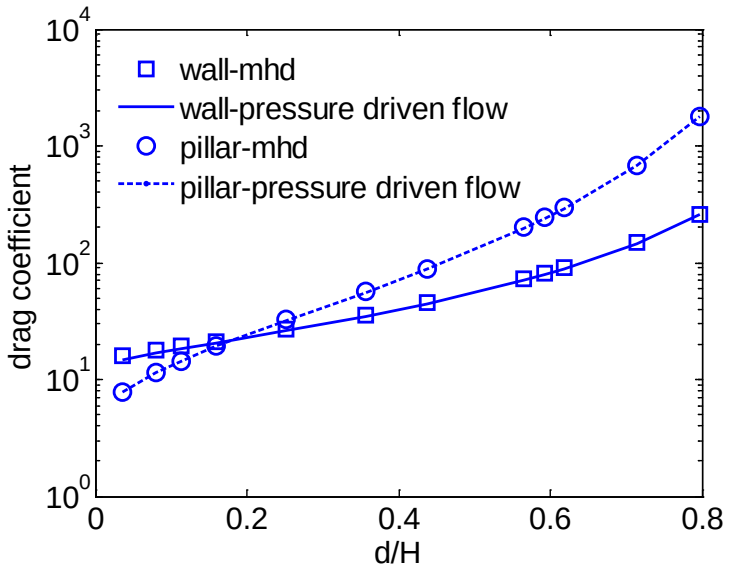

Fig. 8: The drag coefficient at the pillar's surface (dashed line and hollow circles) and at the conduit's surface (solid line and hollow squares) as functions of the pillar's diameter normalized with the conduit's width (H). The lines and symbols correspond, respectively, to pressure-drive flow and the solution of the NP-NS model. For MHD flow, we used $|\mathbf{b}| = 0.4T$, $D_1 = D_3 = 10^{-9} m^2/s$, $D_2 = 4/3 \times 10^{-9} m^2/s$, $z_1 = 3, z_2 = 2, z_3 = -1$, $\overline{c}_1 = \overline{c}_2 = 0.2M$, $\overline{c}_3 = 1M$, $\Delta\hat{V}_{ext} = 25$, $\rho = 10^3 kg/m^3$, $\mu = 10^{-3} Pa \cdot s$, $H = W = 1mm$, $\alpha = 0.5$ and $j_e = 10^{-6} A/m^2$

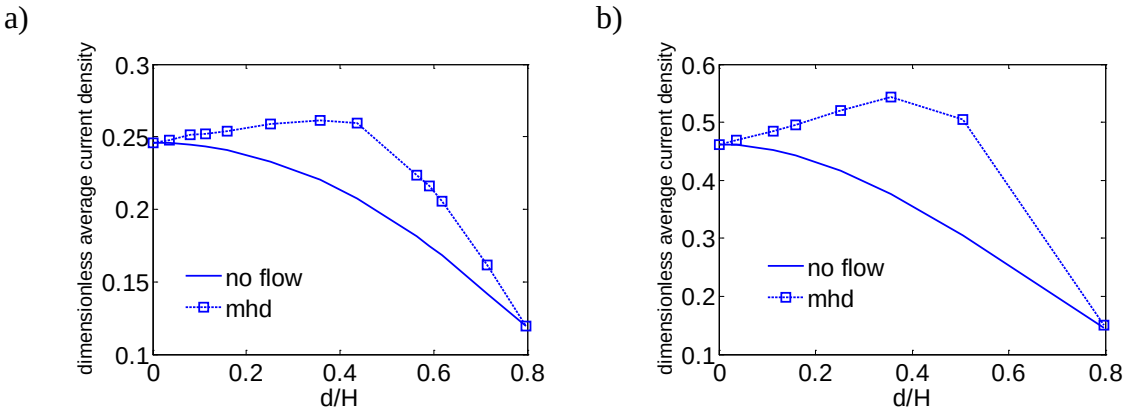

Fig. 9: The average y-component of the dimensionless current flux as a function of d/H in the absence (solid line) and the presence (dashed line with hollow squares) of MHD flow. The potential difference between the electrodes is $\Delta\hat{V}_{ext} = 25$ (a) and 40 (b). All other conditions are the same as in Fig. 8

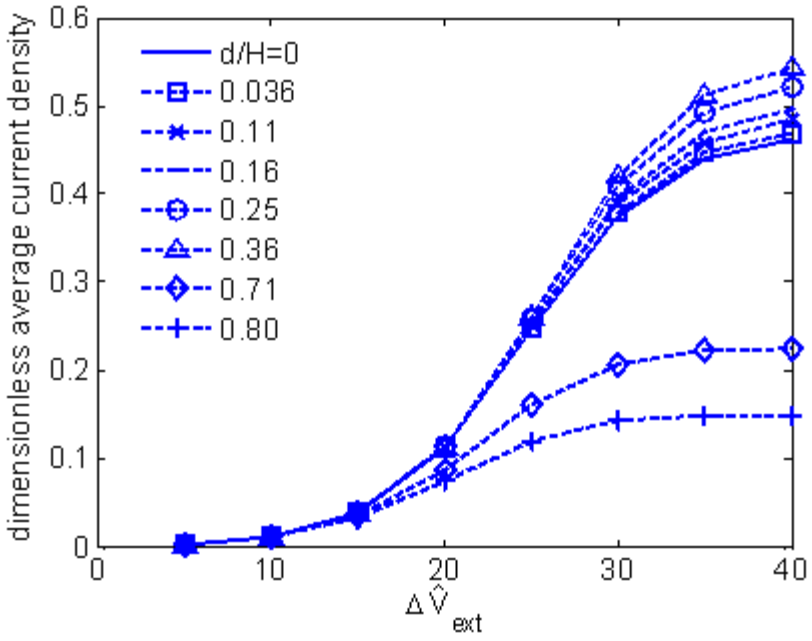

Fig. 10: The average dimensionless current flux $\overline{\hat{j}}_{\hat{y}}$ as a function of the applied dimensionless potential difference $\Delta\hat{V}_{ext}$ when $d/H = 0$, 0.036, 0.11, 0.16, 0.25, 0.36, 0.71 and 0.8. All other conditions are the same as in Fig. 8

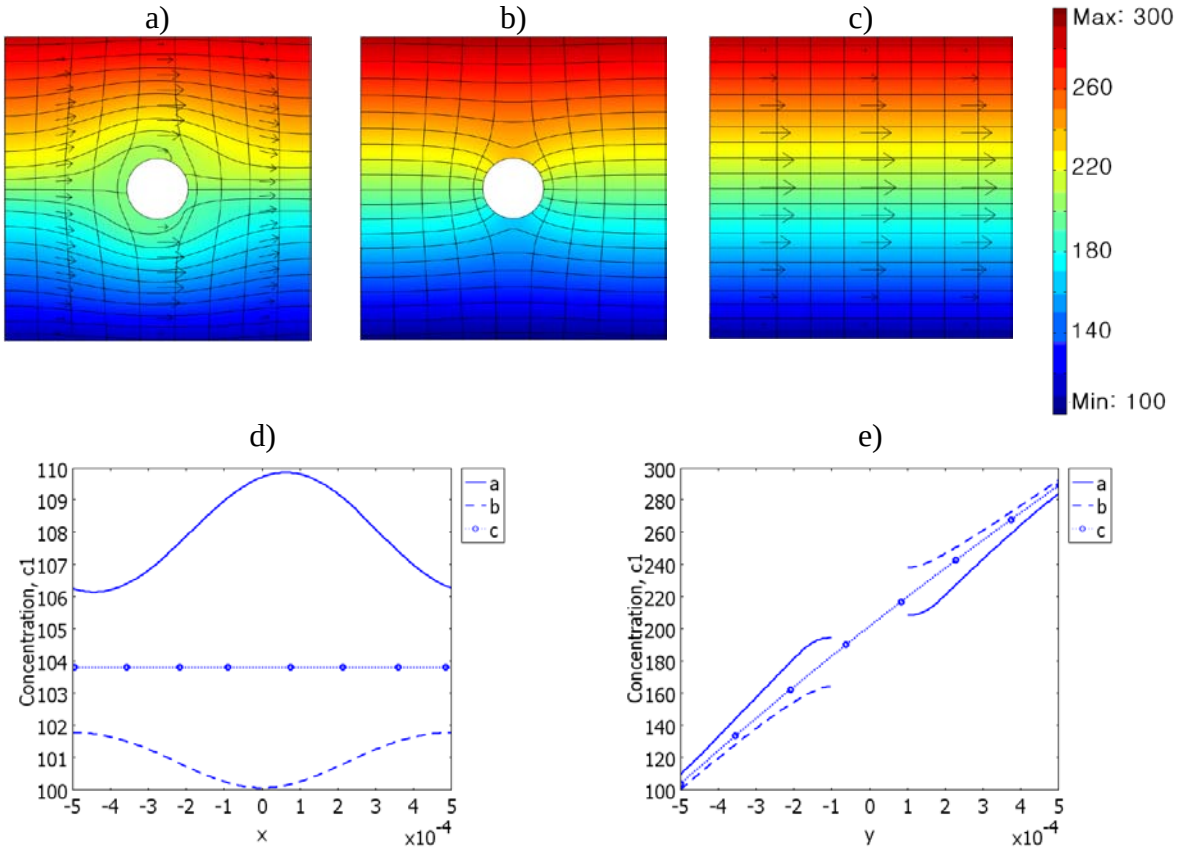

Fig. 11: (a) The concentration field c_1 in the presence of a cylinder ($d/H = 0.2$) and MHD flow. (b) The concentration field for c_1 in the presence of a cylinder ($d/H = 0.2$) and in the absence of motion. (c) The concentration field c_1 in the absence of a cylinder. The color code and the solid longitudinal lines in (a), (b), and (c) correspond, respectively, to concentration and concentration contours. The transverse solid lines are the current fluxes. The arrows are velocity vectors. (d) The concentration distribution $c_1(x,-H/2)$ along the surface of the cathode as a function of x in the presence of motion (solid line), in the absence of the cylinder (dotted line with hollow circles), and in the presence of the cylinder and an absence of motion (dashed line). (e) The concentration distribution $c_1(0,y)$ as a function of y in the presence of motion (solid line), in the absence of the cylinder (dotted line with hollow circles), and in the presence of the cylinder and an absence of motion (dashed line). $\Delta\hat{V}_{ext} = 25$. All other conditions are the same as in Fig. 8

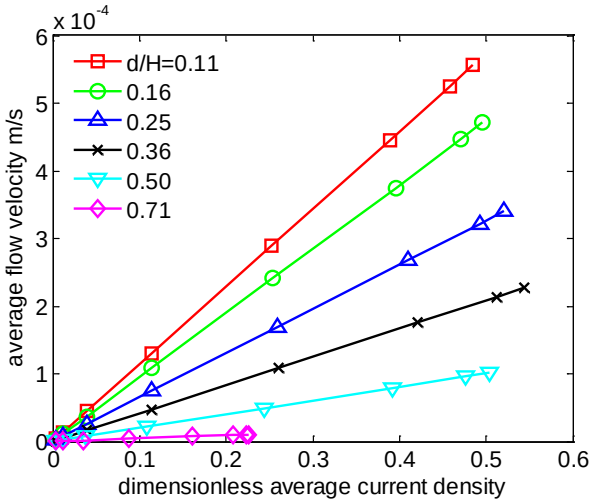

Fig. 12: The average flow velocity $\bar{u}$ as a function of the average dimensionless current $\bar{\hat{j}}_{\hat{y}}$ when $d/H = 0.11$ (square), 0.16 (circle), 0.25 (upright triangle), 0.36 (cross), 0.50 (downward triangle) and 0.71 (diamond). All other conditions are the same as in Fig. 8

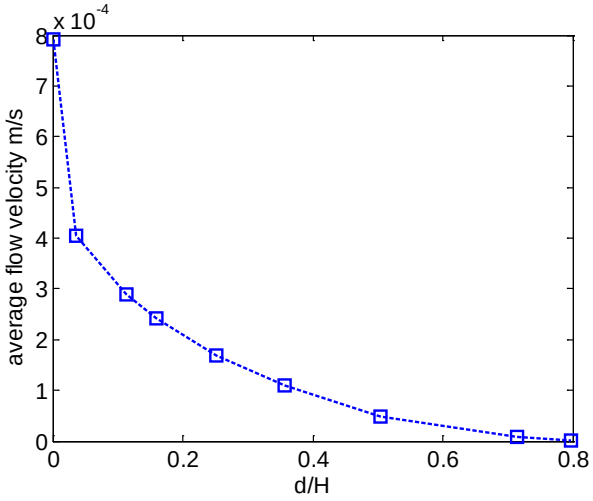

Fig. 13: The average flow velocity $\bar{u}$ as a function of d/H at $\Delta\hat{V}_{ext} = 25$. All other conditions are the same as in Fig. 8. $d/H = 0$ corresponds to an empty straight conduit (in the absence of pillars).